# Fast Whole-Brain Three-dimensional Macromolecular Proton Fraction Mapping in Multiple Sclerosis[1]

Vasily L. Yarnykh, PhD
James D. Bowen, MD
Alexey Samsonov, PhD
Pavle Repovic, MD
Angeli Mayadev, MD
Peiqing Qian, MD
Beena Gangadharan, PhD
Bart P. Keogh, MD, PhD
Kenneth R. Maravilla, MD
Lily K. Jung Henson, MD

**Purpose:** To evaluate the clinical utility of fast whole-brain macromolecular proton fraction (MPF) mapping in multiple sclerosis (MS) and compare MPF with established quantitative magnetic resonance (MR) imaging measures of tissue damage including magnetization transfer (MT) ratio and relaxation rate (R1).

**Materials and Methods:** In this institutional review board–approved and HIPAA-compliant study, 14 healthy control participants, 18 relapsing-remitting MS (RRMS) patients, and 12 secondary progressive MS (SPMS) patients provided written informed consent and underwent 3-T MR imaging. Three-dimensional MPF maps were reconstructed from MT-weighted images and R1 maps by the single-point method. Mean MPF, R1, and MT ratio in normal-appearing white matter (WM), gray matter (GM), and lesions were compared between subject groups by using analysis of variance. Correlations (Pearson *r*) between imaging data and clinical scores (Expanded Disability Status Scale [EDSS] and MS Functional Composite [MSFC]) were compared by using Hotelling-Williams test.

**Results:** RRMS patients had lower WM and GM MPF than controls, with percentage decreases of 6.5% ($P < .005$) and 5.4% ($P < .05$). MPF in SPMS was reduced relative to RRMS in WM, GM, and lesions by 6.4% ($P < .005$), 13.4% ($P < .005$), and 11.7% ($P < .05$), respectively. EDSS and MSFC demonstrated strongest correlations with MPF in GM ($r = -0.74$ and 0.81; $P < .001$) followed by WM ($r = -0.57$ and 0.72; $P < .01$) and lesions ($r = -0.42$ and 0.50; $P < .05$). R1 and MT ratio in all tissues were significantly less correlated with clinical scores than GM MPF ($P < .05$).

**Conclusion:** MPF mapping enables quantitative assessment of demyelination in normal-appearing brain tissues and shows primary clinical relevance of GM damage in MS. MPF outperforms MT ratio and R1 in detection of MS-related tissue changes.



[1] From the Department of Radiology, University of Washington, 1959 NE Pacific St, Seattle, WA 98195 (V.L.Y., K.R.M.); Multiple Sclerosis Center (J.D.B., P.R., A.M., P.Q., B.G., L.K.J.H.) and Department of Radiology (B.P.K.), Swedish Neuroscience Institute, Seattle, Wash; and Department of Radiology, University of Wisconsin, Madison, Wis (A.S.).
From the 2013 RSNA Annual Meeting. Received March 3, 2014; revision requested April 24; revision received May 12; accepted May 20; final version accepted June 11. Supported by the National Multiple Sclerosis Society (grant RG 4864A1/1). **Address correspondence to** V.L.Y. (e-mail: *yarnykh@u.washington.edu*).

Magnetization transfer (MT) magnetic resonance (MR) imaging was widely used in multiple sclerosis (MS) research during the past two decades (1). The majority of studies used MT imaging in its common and technically simplest form based on calculation of the MT ratio that reflects a relative reduction of signal intensity caused by off-resonance radiofrequency saturation of macromolecular protons. The main limitation of this approach is related to a complex dependence of MT ratio on several parameters that describe the MT effect within the two-pool model (2,3). In this model, magnetization dynamics involves cross-relaxation between water and macromolecular protons and relaxation processes within each proton pool. Both relaxation and cross-relaxation parameters contribute to MT ratio, often with opposite effects, which limits its pathologic specificity and dynamic range of disease-related changes (4,5). More complex methods for quantitative mapping of the two-pool model parameters were proposed and tested in several MS studies (6–10). The common limitation of these methods is time-consuming data acquisition because of the need to collect a large number of MT-weighted images at variable saturation parameters. Recently, a new method was developed for fast whole-brain mapping of the macromolecular proton fraction (MPF) (11), a key two-pool model parameter defined as the relative amount of macromolecular protons that determine the MT effect. This method allows MPF measurements in isolation from other two-pool model parameters and requires only one MT-weighted image, reference image, independently acquired map of the longitudinal relaxation rate (R1, or 1/T1), and maps of $B_0$ and $B_1$ fields for inhomogeneity correction.

Practical interest in MPF as a prospective biomarker in MS is driven by a number of recent animal studies (4,5,12–16) that demonstrated strong relationships between MPF and myelin. MPF has been highly positively correlated with histologic measurements of myelin density in animal models, including both normal brain tissues and demyelination (4,12,15,16). Based on quantitative estimates from the literature (5), myelin provides an at least 75% contribution into the MPF measured in white matter (WM). Because it is a disease in which demyelination is a key pathologic substrate of neural tissue damage (17), MS represents a primary area for potential clinical applications of fast MPF mapping.

The objectives of this study were to evaluate the clinical utility of fast whole-brain MPF mapping in MS and compare MPF with established quantitative MR imaging measures of tissue damage including MT ratio and R1.

### Advances in Knowledge

- Macromolecular proton fraction (MPF) is significantly ($P < .05$) reduced in normal-appearing brain tissues of relapsing-remitting multiple sclerosis (MS) patients compared with healthy controls, with a relative decrease of 6.5% in white matter (WM) and 5.4% in gray matter (GM).
- MPF is significantly reduced in both normal-appearing brain tissues ($P < .005$) and lesions ($P < .05$) of secondary progressive MS patients compared with relapsing-remitting MS patients, with the largest relative decrease in GM (13.4%), followed by lesions (11.7%) and WM (6.4%).
- MPF in brain tissues of MS patients significantly correlates with clinical disability evaluated by using Expanded Disability Status Scale and Multiple Sclerosis Functional Composite scores with the strongest associations in GM (respectively, Pearson correlations coefficients: $r = -0.74$ and 0.81; $P < .001$), followed by WM (respectively, $r = -0.57$ and 0.72; $P < .01$), and lesions (respectively, $r = -0.42$ and 0.50; $P < .05$).
- MPF provides more clinically relevant information about pathologic changes in brain tissues than do magnetization transfer ratio, longitudinal relaxation rate, and lesion volume.

### Implication for Patient Care

- Fast whole-brain macromolecular proton fraction mapping can be used to detect demyelination in normal-appearing brain tissues and it provides a promising approach for quantitative monitoring of myelin damage and repair in clinical studies of multiple sclerosis.

## Materials and Methods

### Study Design and Population

This prospective cross-sectional study was approved by the institutional review board and compliant with the Health Insurance Portability and

**Published online before print**
10.1148/radiol.14140528 **Content code:** NR

**Radiology 2015;** 274:210–220

**Abbreviations:**
EDSS = Expanded Disability Status Scale
GM = gray matter
MPF = macromolecular proton fraction
MS = multiple sclerosis
MSFC = MS functional composite
MT = magnetization transfer
PVWGM = partial volume from WM and GM
RRMS = relaxing-remitting MS
SPMS = secondary progressive MS
WM = white matter

**Author contributions:**
Guarantor of integrity of entire study, V.L.Y.; study concepts/study design or data acquisition or data analysis/interpretation, all authors; manuscript drafting or manuscript revision for important intellectual content, all authors; approval of final version of submitted manuscript, all authors; agrees to ensure any questions related to the work are appropriately resolved, all authors; literature research, V.L.Y., P.R.; clinical studies, J.D.B., P.R., A.M., P.Q., B.G., K.R.M., L.K.J.H.; experimental studies, V.L.Y., A.S., B.P.K.; statistical analysis, V.L.Y.; and manuscript editing, V.L.Y., J.D.B., A.S., P.R., A.M., P.Q., K.R.M., L.K.J.H.

**Funding:**
This research was supported by the National Institutes of Health (grants R21EB009908, R21EB016135, and R01NS065034).

Conflicts of interest are listed at the end of this article.

**Table 1**

**MR Imaging Protocol Parameters**

| Parameter | 3D MT-weighted Gradient Echo | 3D Reference Gradient Echo | 3D VFA Gradient-Echo R1 Mapping | 3D Dual Gradient-Echo $B_0$ Mapping | 3D AFI $B_1$ Mapping | 2D T2-weighted FLAIR* |
|---|---|---|---|---|---|---|
| Repetition time(s) (msec) | 43 | 43 | 20 | 20 | 30, 120 | 10000 |
| Echo time(s) (msec) | 2.3 | 2.3 | 2.3 | 2.3; 3.3 | 2.3 | 135 |
| Flip angle(s) (degrees) | 10 | 10 | 3; 10; 20 | 10 | 60 | 90 |
| Saturation pulse offset frequency (kHz)† | 4 | 100‡ | NA | NA | NA | NA |
| Field of view ($mm^2$) | 240 × 180 | 240 × 180 | 240 × 180 | 240 × 180 | 240 × 180 | 240 × 180 |
| Acquired in-plane resolution ($mm^2$) | 1.5 × 1.5 | 1.5 × 1.5 | 1.5 × 1.5 | 1.5 × 3.0 | 1.5 × 3.0 | 1.0 × 1.0 |
| Reconstructed in-plane resolution ($mm^2$) | 1.0 × 1.0 | 1.0 × 1.0 | 1.0 × 1.0 | 1.0 × 1.0 | 1.0 × 1.0 | 1.0 × 1.0 |
| Acquired section thickness (mm) | 4 | 4 | 4 | 4 | 4 | 4 |
| Reconstructed section thickness (mm) | 2 | 2 | 2 | 2 | 2 | 4 |
| No. of acquired sections | 46 | 46 | 46 | 46 | 46 | 46 |
| No. of reconstructed sections | 92 | 92 | 92 | 92 | 92 | 46 |
| Fractional k-space acquisition factors§ | 0.75, 0.9 | 0.75, 0.9 | 0.75, 0.9 | 1, 1 | 0.6, 0.8 | 1, NA |
| No. of acquired signals | 1 | 1 | 1 | 1 | 1 | 1 |
| Acquisition time (sec) | 177 | 177 | 247 | 109 | 212 | 300 |

Note.— AFI = actual flip-angle imaging, FLAIR = fluid-attenuated inversion-recovery, NA = not applicable , 3D = three-dimensional, 2D = two-dimensional, VFA = variable flip angle.

* Inversion time, 2600 msec.

† Off-resonance saturation pulse with single-lobe sinc-Gauss shape, duration of 19 msec, and effective flip angle of 950° was used.

‡ Saturation pulse with the offset frequency at which the MT effect is absent was applied to enable imager's hardware to operate at power settings identical to those for the MT-weighted sequence.

§ Numbers correspond to left-right and foot-head phase-encoding directions.

Accountability Act. Written informed consent was obtained from all participants. Inclusion criteria for MS patients were as follows: age range, 18–70 years; MS diagnosis according to the revised McDonald criteria (18); either relapsing-remitting MS (RRMS) or secondary progressive MS (SPMS) disease course; the absence of relapses within 2 months before study entry; and the absence of neurologic conditions other than MS. Inclusion criteria for control participants were the same age range and the absence of self-reported history of any neurologic disease, brain injury, or substance abuse. Exclusion criteria for all participants were any contraindications to MR imaging, inability to tolerate the MR imaging procedure, and self-withdrawal from the study. Participants were consecutively recruited between April 2010 and November 2012 based on their willingness to take part in the study. Within 1 week before MR imaging, MS patients underwent clinical examination to determine Expanded Disability Status Scale (EDSS) (19) and MS Functional Composite (MSFC) (20) scores. EDSS scoring was performed by a clinical neurologist with at least 6 years of experience (J.D.B., P.R., A.M., P.Q., and L.K.J.H.). Individual components of the MSFC score, including the 25-foot timed walk test, nine-hole peg test, and paced auditory serial addition test with 3-second interstimulus intervals, were administered by a trained evaluator with 4 years of experience (B.G.). In total, 15 control participants and 32 MS patients were recruited. One control participant was excluded because of claustrophobia and two MS patients were excluded because they withdrew themselves from the study. Therefore, the study population included 14 control participants and 30 MS patients.

### MR Imaging Protocol

Images were acquired by using a 3-T imager (Achieva; Philips Medical Systems, Best, the Netherlands) with manufacturer's transmit-receive head coil. A fast three-dimensional whole-brain MPF mapping protocol was implemented as previously described (11), and it included the following sequences applied in the transverse plane: MT-weighted gradient-echo with off-resonance saturation, reference gradient-echo with the same parameters and without MT saturation, three gradient-echo sequences for variable flip-angle R1 mapping, dual gradient-echo for $B_0$ field mapping (21), and actual flip-angle imaging (22) for $B_1$ field mapping. All sequences were implemented with optimized gradient and radiofrequency spoiling (23). Acquisition time for the entire MPF mapping protocol was about 16 minutes. Additionally, two-dimensional T2-weighted fluid-attenuated inversion-recovery images were acquired with matched geometry and contiguous sections for lesion segmentation. Details of imaging sequences are provided in Table 1.

### Image Processing and Analysis

MPF maps were reconstructed by using a previously described single-point method implemented in custom-written C language software by one author with 14-year experience in image processing (V.L.Y.). The reconstruction algorithm is detailed in Figure 1. Before reconstruction, non-brain tissues were removed from source images by applying

**Figure 1**

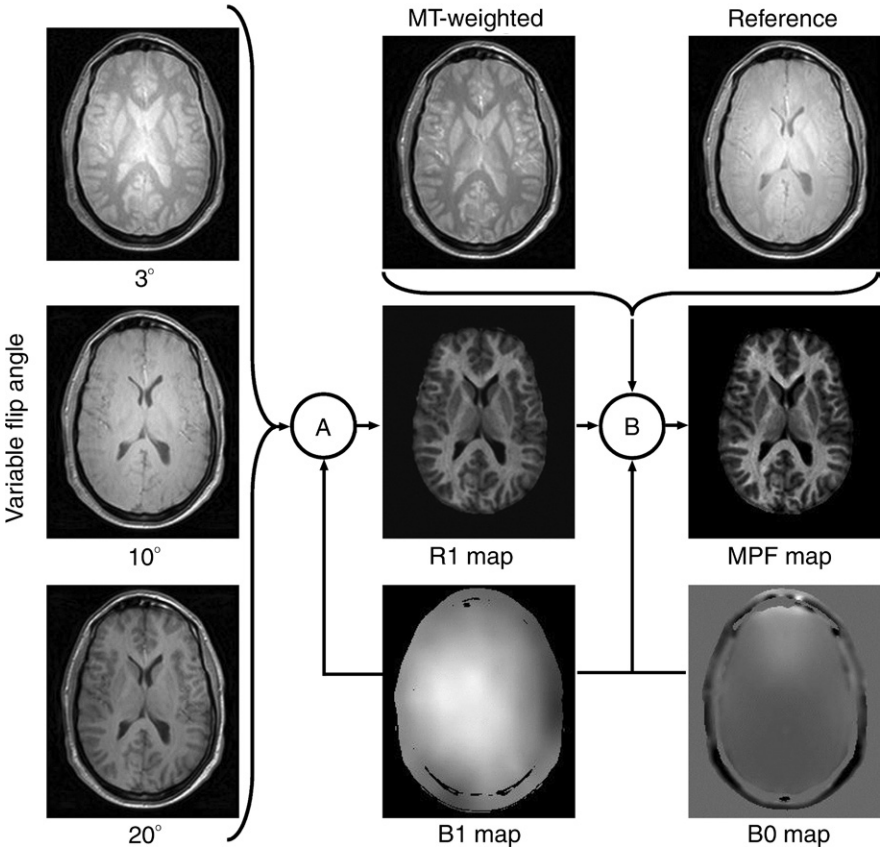


**Figure 1:** Overview of image processing in the fast MPF mapping method (11). Source data include three gradient-echo images for variable flip angle R1 mapping, MT-weighted gradient-echo image with off-resonance saturation, reference gradient-echo image, $B_0$ map, and $B_1$ map. Reconstruction procedure consists of two image processing steps, *(A)* and *(B)*. During the first step *(A)*, the fit of the Ernst equation to variable flip angle data with $B_1$ correction (22) is performed to obtain an R1 map. An R1 map, an MT-weighted image normalized to a reference image, and field maps are used as input data for the second step *(B)*. During this step, the pulsed MT matrix equation (11) is iteratively solved by the Gauss-Newton method with standardized constraints for nonadjustable two-pool model parameters and corrections for $B_0$ and $B_1$ inhomogeneities to create an MPF map.

a brain mask created from the reference image by using freely available software (Functional Magnetic Resonance Imaging of the Brain Software Library; Oxford Centre for Functional Magnetic Resonance Imaging of the Brain, University of Oxford, Oxford, England) (24). Additionally, cerebrospinal fluid was segmented out from R1 maps based on a threshold value of 0.33 $sec^{-1}$ (T1 = 3000 msec). MT ratio maps were computed from MT-weighted and reference images as MT ratio = 100 ($S_{ref}$ − $S_{MT}$) ÷ $S_{ref}$, where $S_{ref}$ and $S_{MT}$ are the signal intensities of the reference and MT-weighted images, respectively. Resulting MPF, R1, and MT ratio maps are shown in Figure 2.

MS lesions were segmented with a semiautomated algorithm by using commercially available software (Jim; Xinapse Systems, Aldwincle, England) from fluid-attenuated inversion-recovery images after interpolation in the section direction to match section thickness of MPF maps. One operator with 7 years of experience (A.S.) was blinded to clinical and other imaging data and performed placement of seed markers to initialize lesion search.

Because of high contrast between WM and gray matter (GM) (Fig 2), MPF maps were used as source images for segmentation of these tissues. Segmentation was performed by an automated segmentation tool by using FSL software (24). To take into account partial volume effects, four tissue classes were prescribed within the single-channel segmentation procedure. These classes correspond to pure WM, pure GM, mixed voxels that contained partial volumes from WM and GM (PVWGM), and mixed voxels that contained a partial volume from cerebrospinal fluid. The latter tissue class was used to correct for potentially incomplete cerebrospinal fluid segmentation by R1 threshold and excluded from subsequent analyses, while the other tissue classes covered the entire brain parenchyma. Because MS lesions may fall into any of the above automatically generated tissue classes, lesion masks were excluded from other tissue masks. The binary segmentation masks were used to calculate mean MPF, R1, and MT ratio in each tissue.

### Statistical Methods

Statistical analysis was performed by using commercially available software (SPSS; SPSS, Chicago, Ill). Data normality within participant groups was assessed by using Shapiro-Wilk test to select an appropriate parametric or nonparametric analysis. Mean parameter values in normal-appearing brain tissues and age were compared between three participant groups (control, RRMS, and SPMS) by using one-way analysis of variance followed by post hoc pairwise tests with Bonferroni adjustments. Clinical variables and mean MR imaging parameters in lesions were compared between RRMS and SPMS patients by using unpaired *t* test or Mann-Whitney *U* test. Differences in sex distribution were assessed by using the Pearson $\chi^2$ test. Distinctions in imaging variables between participant groups (RRMS vs controls and SPMS vs RRMS) were described by percentage differences and effect sizes (Cohen *d*) calculated as the ratio of the mean difference to the pooled standard

deviation. Correlations between imaging and clinical data were investigated by using bivariate linear regression. Shapiro-Wilk test was used to assess normality of residuals, and an appropriate variable transformation was used to correct for significant deviations from normality if detected. For regressions with normally distributed residuals, Pearson correlation coefficients ($r$) were reported. After identification of the strongest significant correlation for each clinical variable, the correlation was compared with correlations between the same clinical variable and other imaging variables by using Hotelling-Williams test. Linear regression was also used to assess relationships between quantitative imaging variables within each tissue class. $P$ values less than .05 were considered to indicate significant differences. Two-tailed tests were used in all analyses except for comparison between correlation coefficients, where one-tailed hypothesis was justified by the observed unidirectional trend.

## Results

### Clinical Data

Clinical and demographic characteristics of study participants are summarized in Table 2. Of the 30 MS patients, 18 patients had RRMS and 12 patients had SPMS disease course. Sex distribution was not significantly different between the groups. There were no significant differences in age both between controls and RRMS patients and between RRMS and SPMS patients, but a significant distinction was found between SPMS patients and controls. SPMS patients had significantly longer disease duration, greater disability as indicated by higher EDSS and lower MSFC scores, and larger lesion volume than RRMS patients.

### Comparison of Quantitative MR Imaging Parameters between Groups

Example segmentation results are presented in Figure 2. Mean MPF, R1, and MT ratio values in segmented brain tissues for all participant groups are

**Figure 2**

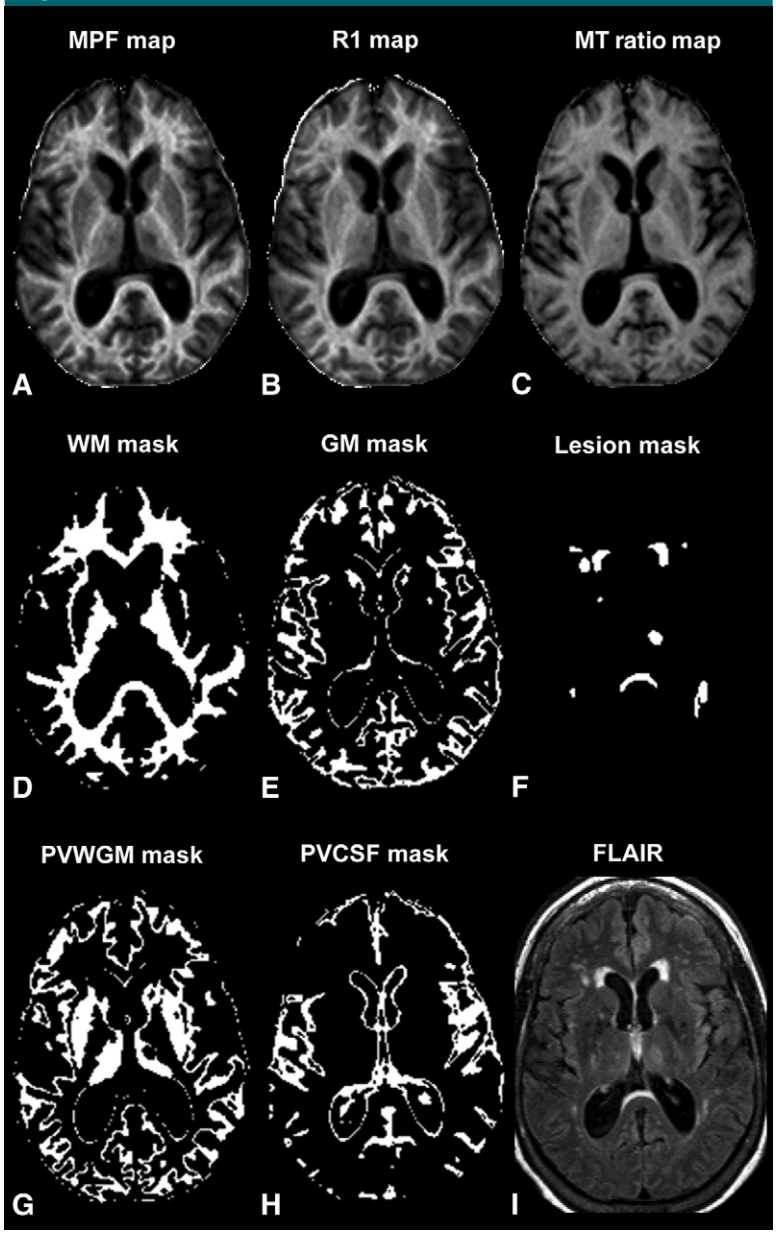


**Figure 2:** Images show example axial sections of, *A*, three-dimensional MPF, *B*, R1, and, *C*, MT ratio parametric maps, *D–H*, corresponding binary tissue segmentation masks, and, *I*, a fluid-attenuated inversion-recovery *(FLAIR)* image used for lesion segmentation, obtained from a 63-year old woman with SPMS disease course. Gray scale windows for parametric maps correspond to parameter ranges as follows: MPF of 0%–20% *(A)*, R1 of 0.3–1.5 $sec^{-1}$ *(B)*, and MT ratio of 10%–60% *(C)*. Segmentation masks correspond to the following tissue classes: WM *(D)*, GM *(E)*, lesions *(F)*, PVWGM *(G)*, and partial volume from cerebrospinal fluid *(PVCSF) (H)*. Four-tissue MPF map segmentation results in conservative masks for normal-appearing WM *(D)* and GM *(E)*, while partial volume effects are absorbed by the neighboring mixed tissues (PVWGM *[G]* and PVCSF *[H]*). Note that that the PVWGM tissue class *(G)* includes both WM-GM junction and subcortical nuclei with relatively high myelin content, whereas pure GM class *(E)* mainly corresponds to less myelinated cortical GM.

**Table 2**

**Clinical and Demographic Characteristics of the Study Population**

| Variable | Control Participants | RRMS Patients | SPMS Patients |
|---|---|---|---|
| No. of participants | 14 | 18 | 12 |
| No. of women | 7 | 12 | 7 |
| No. of men | 7 | 6 | 5 |
| Age (y) | 43.6 ± 10.6 (28–64) | 48.2 ± 10.8 (30–62) | 56.0 ± 6.8 (42–67)* |
| Disease duration (y) | NA | 6.7 ± 3.6 (2–14) | 15.5 ± 7.9 (5–28)† |
| EDSS score | NA | 2.9 ± 1.8 (1.0–6.5) | 6.7 ± 0.8 (5.5–8.0)†‡ |
| MSFC score | NA | 0.49 ± 0.34 (−0.09 to 1.08) | −0.70 ± 0.86 (−2.33 to 0.55)† |
| Lesion volume (mL) | NA | 6.9 ± 6.4 (0.4–24.1) | 20.7 ± 17.0 (4.6–65.0)†‡ |

Note.—Except where indicated, data are mean ± standard deviation. Data in parentheses are range. NA = not applicable.

* Significantly different from control participants.

† Significantly different from RRMS patients.

‡ Mann-Whitney *U* test.

**Table 3**

**Mean Quantitative MR Imaging Variables in Segmented Brain Tissues**

| Variable | Control Participants | RRMS Patients | SPMS Patients |
|---|---|---|---|
| MPF in WM (%) | 13.48 ± 0.37 | 12.61 ± 0.62* | 11.80 ± 0.77*† |
| MPF in GM (%) | 5.77 ± 0.34 | 5.46 ± 0.27* | 4.73 ± 0.39*† |
| MPF in PVWGM (%) | 8.96 ± 0.34 | 8.41 ± 0.42* | 7.61 ± 0.50*† |
| MPF in lesions (%) | NA | 8.48 ± 0.80 | 7.49 ± 0.98† |
| R1 in WM ($sec^{-1}$) | 0.997 ± 0.019 | 0.964 ± 0.031* | 0.932 ± 0.047*† |
| R1 in GM ($sec^{-1}$) | 0.630 ± 0.020 | 0.617 ± 0.023 | 0.597 ± 0.022* |
| R1 in PVWGM ($sec^{-1}$) | 0.773 ± 0.018 | 0.752 ± 0.026 | 0.724 ± 0.030*† |
| R1 in lesions ($sec^{-1}$) | NA | 0.768 ± 0.048 | 0.719 ± 0.048† |
| MT ratio in WM (%) | 38.28 ± 1.27 | 38.22 ± 1.23 | 37.38 ± 2.01 |
| MT ratio in GM (%) | 25.67 ± 1.49 | 25.57 ± 1.17 | 23.50 ± 1.91*† |
| MT ratio in PVWGM (%) | 32.12 ± 1.31 | 31.95 ± 1.15 | 30.57 ± 1.94*† |
| MT ratio in lesions (%) | NA | 31.99 ± 1.85 | 30.33 ± 2.44† |

Note.—Data are mean ± standard deviation. Bonferroni correction for three-group comparisons was used where applicable. NA = not applicable.

* Significantly different from control participants.

† Significantly different from RRMS patients.

summarized in Table 3. No significant deviations from the normal distribution were found in any of quantitative imaging variables. Effects of age and sex and their interactions with the group factor were tested by using the general linear model analysis of variance and the effects were found to be nonsignificant. Both RRMS and SPMS patients had significantly reduced MPF compared with controls in WM, GM, and mixed PVWGM tissues. SPMS patients had significantly lower MPF than RRMS patients in all normal-appearing tissues and lesions. Compared with controls, R1 in RRMS patients was significantly decreased in WM but not in GM and mixed PVWGM tissue. The significant R1 distinctions between RRMS and SPMS patients were found in WM, PVWGM, and lesions, whereas the difference in GM was not significant. MT ratio in all tissues failed to distinguish between RRMS patients and controls. SPMS patients had significantly reduced MT ratio compared with RRMS in GM, PVWGM, and lesions, but not in WM.

Relative changes in MR imaging parameters between participant groups and associated effect sizes (Cohen *d*) are summarized in Figure 3. MPF in WM demonstrated the largest decrease in RRMS patients compared with controls in terms of both percentage change and effect size. However, MPF in GM provided the largest percentage decrease and corresponding effect size for SPMS patients relative to RRMS patients. It is noticeable that a relative decrease of MPF in GM for SPMS patients compared with RRMS is about twofold larger than that in WM, whereas both parameters have close percentage changes in RRMS patients relative to controls. The percentage decreases and effect sizes for MPF in the mixed PVWGM tissue exhibited intermediate values between those in pure WM and GM. In each tissue type, R1 and MT ratio showed consistently smaller percentage differences between groups and effect sizes than MPF.

### Correlations between Clinical and Imaging Data

Correlation coefficients that describe bivariate associations between clinical and imaging variables in the whole group of MS patients are listed in Table 4. Highly significant correlations were identified between MPF in all normal-appearing tissues and clinical variables including disease duration, EDSS MSFC score, and its components. No significant correlations were found between age and any of the imaging variables. MPF in GM demonstrated the strongest correlations with all clinical variables, followed by MPF in mixed PVWGM tissue and WM. Plots of regressions of MPF in GM versus EDSS and MSFC scores are shown in Figure 4. Correlations between MPF in lesions and clinical scores were consistently weaker, and the correlation of this parameter with the disease duration was not significant. MPF in GM showed

**Figure 3**

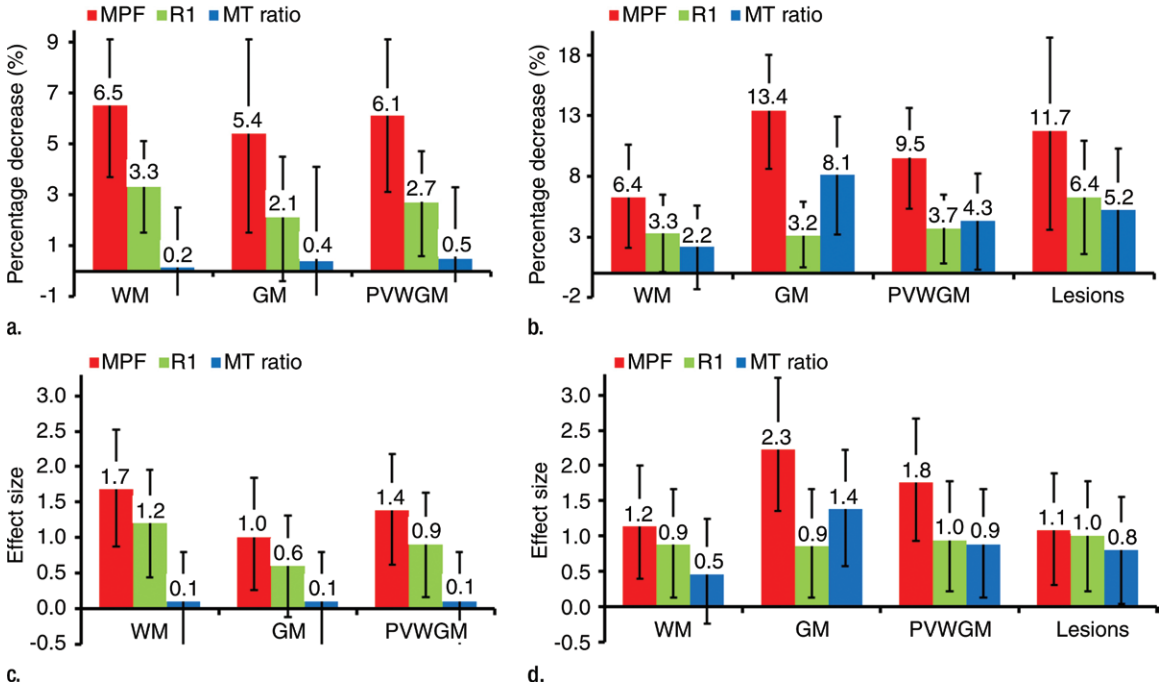


**Figure 3:** Graphs show percentage differences in quantitative imaging parameters between participant groups and associated effect sizes (Cohen *d*). Bar diagrams and numbers above the bars correspond to **(a)** percentage decreases in RRMS patients relative to controls, **(b)** percentage decreases in SPMS patients relative to RRMS patients, **(c)** effect sizes for difference between controls and RRMS patients, and **(d)** effect sizes for difference between RRMS patients and SPMS patients. Error bars correspond to 95% confidence intervals. In each tissue class (WM, GM, PVWGM, and lesions), MPF provides larger distinctions between subject groups than R1 and MT ratio. MPF in WM has the largest percentage change and effect size between controls and RRMS patients. MPF in GM has the largest percentage change and effect size between RRMS and SPMS patients.

significantly stronger association with EDSS, 25-foot timed walk test, and paced auditory serial addition test scores than MPF in WM and lesions according to Hotelling-Williams test. While the similar trend was observed for the disease duration, MSFC score, and nine-hole peg test score, significance of the difference between correlation coefficients was achieved only for MPF in lesions. Individual components of the MSFC score were characterized by generally similar to the composite score patterns of correlations with slightly smaller correlation coefficients. There was no clear dominance of any individual MSFC component, although correlations were slightly stronger for the tests associated with motor function (25-foot timed walk test and nine-hole peg test) than for the cognitive paced auditory serial addition test.

R1 in normal-appearing tissues were weakly to moderately correlated with disease duration, MSFC score, and its components, but significance was not reached for the correlations between R1 and EDSS in all tissues and nine-hole peg test and paced auditory serial addition test scores in GM. R1 in lesions significantly correlated only with MSFC score and its components. MT ratio showed a qualitatively similar to MPF pattern of correlations with clinical variables including the strongest relationship in GM followed by PVWGM, WM, and lesions. At the same time, correlation coefficients for MT ratio in each tissue type with each clinical variable were consistently smaller in absolute value than those for MPF. Lesion volume showed moderate correlations with all clinical variables. Quantitative comparison between correlation coefficients (Hotelling-Williams test) demonstrated that R1 and MT ratio in any tissue type and lesion volume were significantly weaker associated with any of the clinical variables (except for the correlations between MT ratio and nine-hole peg test score) than MPF in GM (Table 4).

## Correlations between Quantitative Imaging Variables

R1 and MT ratio significantly correlated with MPF within each tissue class ($P < .001$). Selected correlation plots are shown in Figure 5. R1 was strongly correlated with MPF in WM ($r = 0.85$), whereas a weaker correlation was found in GM ($r = 0.59$). MT ratio showed an opposite trend, and was stronger correlated with MPF in GM ($r = 0.82$) than in WM ($r = 0.52$). Correlations with MPF in mixed PVWGM

**Table 4**

**Correlations between Imaging and Clinical Variables in MS Patients**

| | Clinical Variable | | | | | | |
|---|---|---|---|---|---|---|---|
| Imaging Variable | Age | Disease Duration | EDSS Score | MSFC Score | 25-foot Timed Walk Test Score | Nine-hole Peg Test Score | Paced Auditory Serial Addition Test Score |
| MPF in WM | −0.27 | −0.54* | −0.57*† | 0.72* | −0.57*† | −0.70* | 0.55*† |
| MPF in GM | −0.34 | −0.67*‡ | −0.74*‡ | 0.81*‡ | −0.75*‡ | −0.78*‡ | 0.71*‡ |
| MPF in PVWGM | −0.29 | −0.60* | −0.65*† | 0.78* | −0.64*† | −0.77* | 0.64* |
| MPF in lesions | −0.11 | −0.32† | −0.42*† | 0.50*† | −0.48*† | −0.52*† | 0.41*† |
| R1 in WM | −0.20 | −0.43*† | −0.33† | 0.56*† | −0.46*† | −0.47*† | 0.39*† |
| R1 in GM | −0.02 | −0.39*† | −0.27† | 0.41*† | −0.44*† | −0.34† | 0.22† |
| R1 in PVWGM | −0.12 | −0.42*† | −0.33† | 0.56*† | −0.47*† | −0.48*† | 0.40*† |
| R1 in lesions | −0.18 | −0.32† | −0.28† | 0.46*† | −0.41*† | −0.42*† | 0.42*† |
| MT ratio in WM | −0.21 | −0.34† | −0.42*† | 0.54*† | −0.37*† | −0.63* | 0.39*† |
| MT ratio in GM | −0.36 | −0.51*† | −0.62*† | 0.68*† | −0.58*† | −0.72* | 0.59*† |
| MT ratio in PVWGM | −0.29 | −0.41*† | −0.51*† | 0.62*† | −0.47*† | −0.69* | 0.50*† |
| MT ratio in lesions | −0.03 | −0.22† | −0.38*† | 0.42*† | −0.39*† | −0.51*† | 0.31† |
| Lesion volume | 0.20 | 0.46*† | 0.49*† | −0.57*† | 0.53*† | 0.47*† | −0.48*† |

Note.—Data are Pearson correlation coefficients. To correct for deviations from normal distribution, Box-Cox transformation was applied to the 25-foot timed walk test score, nine-hole peg test score, and lesion volume with the power of −0.5, −0.5, and 0.5, respectively.

* Significant correlations.

† Correlation coefficient is significantly different from the correlation coefficient with the largest significant absolute value for the same clinical variable based on Hotelling-Williams test.

‡ Correlation coefficient with the largest significant absolute value for a particular clinical variable.

tissue were intermediate between those in WM and GM for both R1 ($r$ = 0.79) and MT ratio ($r$ = 0.69). In lesions, both R1 ($r$ = 0.87) and MT ratio ($r$ = 0.89) strongly correlated with MPF (Fig 5). Correlations between R1 and MT ratio were weak in normal-appearing tissues (WM: $r$ = 0.36, $P$ = .02; GM: $r$ = 0.32, $P$ = .03; and PVWGM: $r$ = 0.43, $P$ = .004) and stronger in lesions ($r$ = 0.67, $P$ < .001).

**Figure 4**

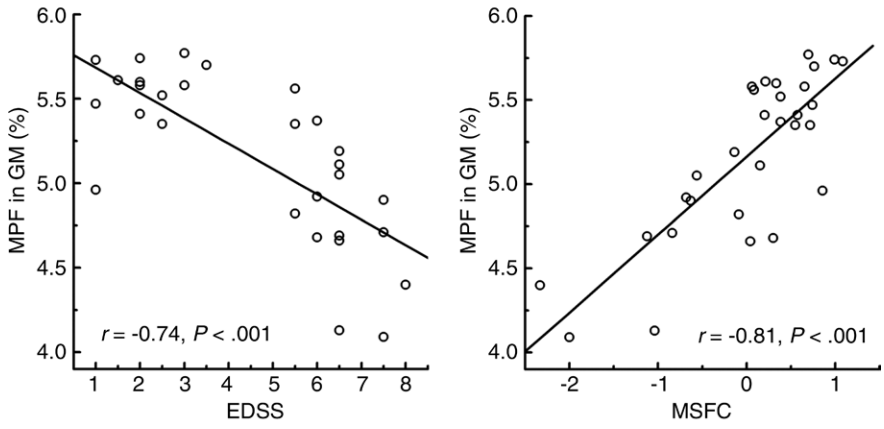


**Figure 4:** Scatterplots show MPF in GM versus **(a)** EDSS and **(b)** MSFC clinical scores. The lines depict linear regression plots, and the numbers are Pearson correlation coefficients *(r)* and *P* values. MPF in GM demonstrated the strongest correlations with both clinical scores across all imaging variables.

## Discussion

The key finding of this study is the high clinical relevance of MPF in GM, which showed the strongest correlations with clinical scores and the largest distinction related to disease course. Notably, MPF in SPMS patients was disproportionally reduced in GM compared with WM. Our observations are in line with the pathologic evidence of strikingly increased cortical demyelination in progressive MS compared with RRMS (25), and they emphasize the critical role of GM damage for disease progression (17,26). While MPF in WM showed a weaker relationship to disability than MPF in GM, it provided a better capability to discriminate between RRMS patients and controls. This finding suggests that demyelination in WM may be more pronounced at earlier stages of the disease compared with GM, and MPF in WM could be a more appropriate target to monitor therapeutic effects in early MS. Unlike normal-appearing brain tissues, MPF in lesions demonstrated substantially weaker

**Figure 5**

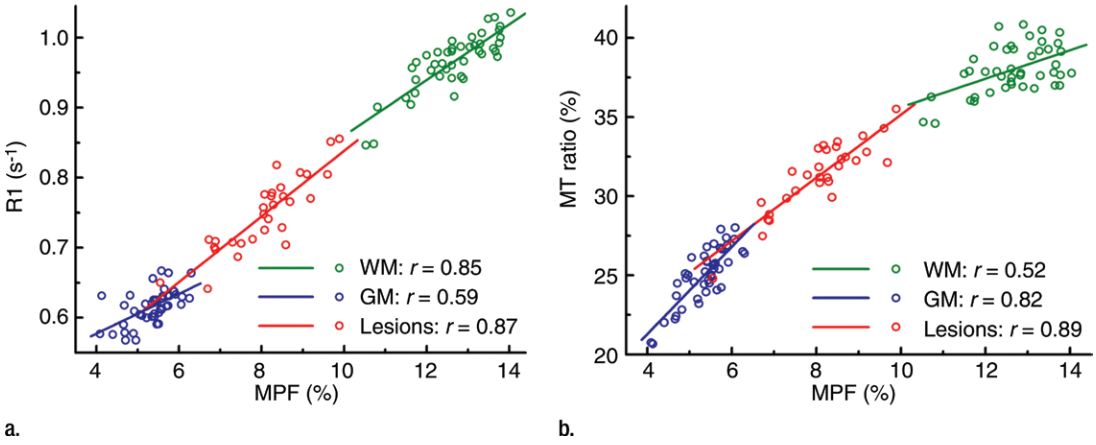


a. b.

**Figure 5:** Scatterplots show **(a)** R1 and **(b)** MT ratio versus MPF. The lines depict linear regression plots and the numbers are Pearson correlation coefficients *(r)*. All correlations are significant ($P < .001$). WM and GM data are plotted for all participants, including MS patients and healthy participants. R1 correlates more strongly with MPF in WM than in GM, whereas MT ratio correlates more strongly with MPF in GM than in WM.

associations with clinical scores, similar to the lesion volume, despite a large percentage decrease in SPMS compared with RRMS. Lesion volume is known to poorly correlate with disability in MS (27). Correlations between lesion volume and clinical scales in this study were on the high end of the range reported in the literature (27), probably because of a wide spectrum of disability in our patient population. A limited capability of both lesion volume and MPF in lesions to explain clinical status supports the current understanding of MS as a whole-brain disease in which widespread microscopic demyelination in normal-appearing tissues mainly determines progression of disability (17,28).

A decrease of MPF in all brain tissues is generally consistent with progressive demyelination as the primary pathologic substrate of neural tissue damage in MS (17) and strong associations between MPF and myelin content established in animal models (4,5,12–16). While microscopic myelin damage is probably the dominant cause of MPF reduction in normal-appearing WM, pathologic changes of MPF in MS lesions may also be driven by edema associated with inflammation because an increase in water content causes dilution of the total macromolecular concentration. Notably, contributions of edema and demyelination can be separated by using a combination of MPF and quantitative proton density mapping (8,10). This approach showed that the loss of myelin is the main reason for MPF changes, even in acute MS lesions (10). Another important issue consequent to our findings is whether demyelination is a sole mechanism of MPF reduction in GM. While the myelin content in GM is much lower compared with WM, a relative change of MPF in GM is close (for RRMS) or higher (for SPMS) than that in WM. This translates to a larger degree of myelin loss in GM compared with WM in both RRMS and SPMS, if MPF changes are assumed to be entirely because of demyelination. Such a difference may have several explanations. First, global GM MPF measurements in our study contained contributions from both GM lesions and normal-appearing tissue because of low sensitivity of the fluid-attenuated inversion-recovery sequence to GM lesions (29). Although GM lesions are known to be less inflammatory than WM lesions (30), some effect of inflammation still can be present (31). Pathologic evidence suggests that GM lesion volume can be rather extensive and approach 70% of the cortex in extreme cases (25,32). Second, GM in MS indeed may be more demyelinated than WM according to pathologic data (32). Finally, MPF changes in GM may be caused by a combined effect of demyelination and neurodegeneration. Specifically, GM is characterized by high density of neuronal plasma membranes because of dendritic arborization. Plasma membranes represent complex lipoprotein structures with a large concentration of the semisolid proton pool involved in the MT effect (33), and therefore they may provide a major nonmyelin contribution into MPF. Accordingly, in the absence of myelin, GM has a larger MPF than WM, as it was reported for the canine mutant demyelination model (4.6% in GM vs 3.1% in WM [5]). Neurodegeneration results in elimination of a portion of membrane material because of the neuronal, synaptic, and glial loss (34), which may additionally contribute to a decrease of MPF. Within this interpretation, our observations are in agreement with the current view of MS as a two-phase disease, where the inflammatory demyelination phase precedes the neurodegenerative phase, which is associated with the progressive clinical course (17). While a detailed elucidation of

possible mechanisms of an MPF reduction in GM can be the subject of future research, our results suggest usefulness of this parameter as an imaging biomarker closely associated with the disease phenotype and severity.

Compared with other quantitative imaging indexes potentially associated with myelin (ie, MT ratio and R1), MPF demonstrated consistently superior performance in both discrimination between participant groups and correlations with clinical scales. Our observations are in overall agreement with sensitivity of MT ratio and R1 to pathologic changes in normal-appearing brain tissues found in earlier studies (1,28,35), and relatively weak (if significant) correlations with disability (36–38) and limited distinctions between patients and controls (38,39). Notably, correlations between these variables and MPF show different patterns within specific brain tissues. Relative strengths of these correlations in conjunction with associations between clinical and imaging data corroborate observed differences in clinical relevance of R1 and MT ratio. A closer association with clinical status of R1 in WM compared with GM can be explained by the fact that R1 in WM is dominated by myelination (40), and therefore varies in a way that is similar to MPF. However, sensitivity of R1 to demyelination in GM is reduced because of low background myelin content and a potential effect of iron accumulation (26). The opposite behavior of MT ratio is in agreement with its theoretical dependence on the two-pool MT model parameters (3). Specifically, simultaneous decreases in MPF and R1 caused by demyelination partially offset each other in WM, which therefore reduces pathologic variability of MT ratio. Conversely, MT ratio provides a better probe of MPF in GM because of smaller R1 variability. Different than in normal-appearing tissues, more collinear variation of MPF, R1, and MT ratio in lesions may be because of several factors, including a wide range of myelin loss, confounding effect of edema, or partial volume averaging with surrounding WM.

This study has several limitations. First, MPF mapping in its current implementation has relatively low spatial resolution. This limitation has been mitigated by the specially designed segmentation procedure, which minimizes partial volume effects and allows conservative parameter estimation for the two tissues of main interest (WM and GM). However, interpretation of pathologic changes in subcortical GM structures, which typically fall within the mixed PVWGM tissue, is difficult because of partial volume averaging. While the reported GM data are representative for cortex, detailed investigations of subcortical GM demyelination is a topic for future studies. It is important to note that MPF mapping has a potential for improvement in resolution without significant imaging time penalties by using parallel imaging. Second, we did not study the role of cortical lesions for MPF reduction in GM. However, it is unlikely that adjustments for cortical lesions could change conclusions of this study because only a small portion of histologic-confirmed GM lesions, which typically correspond to 1%–2% of the cortex volume (41), are detected with MR imaging (29). Third, we did not use a contrast agent to minimize risks to the participants. Further studies that combine higher resolution MPF mapping and contrast enhancement are needed for more comprehensive characterization of demyelination and inflammation in lesions.

In conclusion, this study showed that whole-brain macromolecular proton fraction mapping enables quantitative assessment of demyelination in normal-appearing WM and GM and better correlates with clinical status in multiple sclerosis than traditional magnetization transfer and R1 mapping. Our results demonstrate utility of MPF as a myelin biomarker in MS, reveal primary clinical relevance of GM demyelination, and provide methodologic background for future applications of fast MPF mapping as a clinically targeted tool for quantitative monitoring of myelin damage and repair.

**Disclosures of Conflicts of Interest: V.L.Y.** disclosed no relevant relationships. **J.D.B.** Activities related to the present article: none to disclose. Activities not related to the present article: author receives fees and other from Biogen, EMD Serono, Genentec, Genzyme, GlaxoSmithKline, Medimmune, Novartis, Sanofi-Aventis, Teva Neuroscience, and Pfizer. Other relationships: none to disclose. **A.S.** disclosed no relevant relationships. **P.R.** disclosed no relevant relationships. **A.M.** disclosed no relevant relationships. **P.Q.** disclosed no relevant relationships. **B.G.** disclosed no relevant relationships. **B.P.K.** disclosed no relevant relationships. **K.R.M.** disclosed no relevant relationships. **L.K.J.H.** disclosed no relevant relationships.

## References

1. Filippi M, Rocca MA. Magnetization transfer magnetic resonance imaging of the brain, spinal cord, and optic nerve. Neurotherapeutics 2007;4(3):401–413.
2. Graham SJ, Henkelman RM. Pulsed magnetization transfer imaging: evaluation of technique. Radiology 1999;212(3):903–910.
3. Yarnykh VL. Pulsed Z-spectroscopic imaging of cross-relaxation parameters in tissues for human MRI: theory and clinical applications. Magn Reson Med 2002;47(5):929–939.
4. Underhill HR, Rostomily RC, Mikheev AM, Yuan C, Yarnykh VL. Fast bound pool fraction imaging of the in vivo rat brain: association with myelin content and validation in the C6 glioma model. Neuroimage 2011;54(3):2052–2065.
5. Samsonov A, Alexander AL, Mossahebi P, Wu YC, Duncan ID, Field AS. Quantitative MR imaging of two-pool magnetization transfer model parameters in myelin mutant shaking pup. Neuroimage 2012;62(3):1390–1398.
6. Tozer D, Ramani A, Barker GJ, Davies GR, Miller DH, Tofts PS. Quantitative magnetization transfer mapping of bound protons in multiple sclerosis. Magn Reson Med 2003;50(1):83–91.
7. Davies GR, Tozer DJ, Cercignani M, et al. Estimation of the macromolecular proton fraction and bound pool T2 in multiple sclerosis. Mult Scler 2004;10(6):607–613.
8. Levesque I, Sled JG, Narayanan S, et al. The role of edema and demyelination in chronic T1 black holes: a quantitative magnetization transfer study. J Magn Reson Imaging 2005;21(2):103–110.
9. Narayanan S, Francis SJ, Sled JG, et al. Axonal injury in the cerebral normal-appearing white matter of patients with multiple sclerosis is related to concurrent demyelination

in lesions but not to concurrent demyelination in normal-appearing white matter. Neuroimage 2006;29(2):637–642.

10. Giacomini PS, Levesque IR, Ribeiro L, et al. Measuring demyelination and remyelination in acute multiple sclerosis lesion voxels. Arch Neurol 2009;66(3):375–381.
11. Yarnykh VL. Fast macromolecular proton fraction mapping from a single off-resonance magnetization transfer measurement. Magn Reson Med 2012;68(1):166–178.
12. Odrobina EE, Lam TY, Pun T, Midha R, Stanisz GJ. MR properties of excised neural tissue following experimentally induced demyelination. NMR Biomed 2005;18(5):277–284.
13. Rausch M, Tofts P, Lervik P, et al. Characterization of white matter damage in animal models of multiple sclerosis by magnetization transfer ratio and quantitative mapping of the apparent bound proton fraction f. Mult Scler 2009;15(1):16–27.
14. Ou X, Sun SW, Liang HF, Song SK, Gochberg DF. The MT pool size ratio and the DTI radial diffusivity may reflect the myelination in shiverer and control mice. NMR Biomed 2009;22(5):480–487.
15. Janve VA, Zu Z, Yao SY, et al. The radial diffusivity and magnetization transfer pool size ratio are sensitive markers for demyelination in a rat model of type III multiple sclerosis (MS) lesions. Neuroimage 2013;74:298–305.
16. Thiessen JD, Zhang Y, Zhang H, et al. Quantitative MRI and ultrastructural examination of the cuprizone mouse model of demyelination. NMR Biomed 2013;26(11):1562–1581.
17. Lassmann H, Brück W, Lucchinetti CF. The immunopathology of multiple sclerosis: an overview. Brain Pathol 2007;17(2):210–218.
18. Polman CH, Reingold SC, Banwell B, et al. Diagnostic criteria for multiple sclerosis: 2010 revisions to the McDonald criteria. Ann Neurol 2011;69(2):292–302.
19. Kurtzke JF. Rating neurologic impairment in multiple sclerosis: an expanded disability status scale (EDSS). Neurology 1983;33(11):1444–1452.
20. Fischer JS, Rudick RA, Cutter GR, Reingold SC. The Multiple Sclerosis Functional Composite Measure (MSFC): an integrated approach to MS clinical outcome assessment. National MS Society Clinical Outcomes Assessment Task Force. Mult Scler 1999; 5(4):244–250.
21. Skinner TE, Glover GH. An extended two-point Dixon algorithm for calculating separate water, fat, and B0 images. Magn Reson Med 1997;37(4):628–630.
22. Yarnykh VL. Actual flip-angle imaging in the pulsed steady state: a method for rapid three-dimensional mapping of the transmitted radiofrequency field. Magn Reson Med 2007;57(1):192–200.
23. Yarnykh VL. Optimal radiofrequency and gradient spoiling for improved accuracy of T1 and B1 measurements using fast steady-state techniques. Magn Reson Med 2010;63(6):1610–1626.
24. Smith SM, Jenkinson M, Woolrich MW, et al. Advances in functional and structural MR image analysis and implementation as FSL. Neuroimage 2004;23(Suppl 1): S208–S219.
25. Kutzelnigg A, Lucchinetti CF, Stadelmann C, et al. Cortical demyelination and diffuse white matter injury in multiple sclerosis. Brain 2005;128(Pt 11):2705–2712.
26. Pirko I, Lucchinetti CF, Sriram S, Bakshi R. Gray matter involvement in multiple sclerosis. Neurology 2007;68(9):634–642.
27. Barkhof F. MRI in multiple sclerosis: correlation with expanded disability status scale (EDSS). Mult Scler 1999;5(4):283–286.
28. Filippi M, Rocca MA. MRI evidence for multiple sclerosis as a diffuse disease of the central nervous system. J Neurol 2005;252(Suppl 5): v16–v24.
29. Geurts JJ, Bö L, Pouwels PJ, Castelijns JA, Polman CH, Barkhof F. Cortical lesions in multiple sclerosis: combined postmortem MR imaging and histopathology. AJNR Am J Neuroradiol 2005;26(3):572–577.
30. Bø L, Vedeler CA, Nyland H, Trapp BD, Mørk SJ. Intracortical multiple sclerosis lesions are not associated with increased lymphocyte infiltration. Mult Scler 2003;9(4):323–331.
31. Lucchinetti CF, Popescu BF, Bunyan RF, et al. Inflammatory cortical demyelination in early multiple sclerosis. N Engl J Med 2011; 365(23):2188–2197.
32. Gilmore CP, Donaldson I, Bö L, Owens T, Lowe J, Evangelou N. Regional variations in the extent and pattern of grey matter demyelination in multiple sclerosis: a comparison between the cerebral cortex, cerebellar cortex, deep grey matter nuclei and the spinal cord. J Neurol Neurosurg Psychiatry 2009;80(2):182–187.
33. Bloom M, Holmes KT, Mountford CE, Williams PG. Complete proton magnetic resonance in whole cells. J Magn Reson 1986;69(1): 73–91.
34. Wegner C, Esiri MM, Chance SA, Palace J, Matthews PM. Neocortical neuronal, synaptic, and glial loss in multiple sclerosis. Neurology 2006;67(6):960–967.
35. MacKay AL, Vavasour IM, Rauscher A, et al. MR relaxation in multiple sclerosis. Neuroimaging Clin N Am 2009;19(1):1–26.
36. Vrenken H, Geurts JJ, Knol DL, et al. Whole-brain T1 mapping in multiple sclerosis: global changes of normal-appearing gray and white matter. Radiology 2006;240(3): 811–820.
37. Fisniku LK, Altmann DR, Cercignani M, et al. Magnetization transfer ratio abnormalities reflect clinically relevant grey matter damage in multiple sclerosis. Mult Scler 2009;15(6): 668–677.
38. Vrenken H, Pouwels PJ, Ropele S, et al. Magnetization transfer ratio measurement in multiple sclerosis normal-appearing brain tissue: limited differences with controls but relationships with clinical and MR measures of disease. Mult Scler 2007;13(6): 708–716.
39. Castriota-Scanderbeg A, Fasano F, Filippi M, Caltagirone C. T1 relaxation maps allow differentiation between pathologic tissue subsets in relapsing-remitting and secondary progressive multiple sclerosis. Mult Scler 2004;10(5):556–561.
40. Koenig SH, Brown RD 3rd, Spiller M, Lundbom N. Relaxometry of brain: why white matter appears bright in MRI. Magn Reson Med 1990;14(3):482–495.
41. Calabrese M, Agosta F, Rinaldi F, et al. Cortical lesions and atrophy associated with cognitive impairment in relapsing-remitting multiple sclerosis. Arch Neurol 2009;66(9): 1144–1150.